ACS SENSORS

pubs.acs.org/acssensors

Article

Immunoassays for Extracellular Vesicle Detection via Transmembrane Proteins Using Surface Plasmon Resonance Biosensors

Jesus M. Lopez Baltazar, Wenchao Gu, Markéta Bocková, and Qiuming Yu*

Cite This: https://doi.org/10.1021/acssensors.4c00558

Read Online

ACCESS | Metrics & More | Article Recommendations | Supporting Information

ABSTRACT: Extracellular vesicles (EVs) are preeminent carriers of biomarkers and have become the subject of intense biomedical research for medical diagnostics using biosensors. To create effective EV-based immunoassays, it is imperative to develop surface chemistry approaches with optimal EV detection targeting transmembrane protein biomarkers that are not affected by cell-to-cell variability. Here, we developed a series of immunoassays for the detection of EVs derived from mouse monocyte cells using surface plasmon resonance (SPR) biosensors. We chemically immobilized antibodies onto mixed self-assembled monolayers of oligo ethylene glycol (OEG) alkanethiolates with carboxylic and hydroxylic terminal groups. The effects of antibody clonality (monoclonal vs polyclonal) and antibody surface coverage in targeting EVs via CD81 tetraspanins were investigated. We determined binding kinetic parameters, establishing trends from steric hindrance effects and epitope recognition properties of antibodies. Our results indicate that a 40% surface coverage of polyclonal antibodies covalently linked onto a mixed SAM with 10% of terminated −COOH groups yields a promising approach for EV detection with a linear range of 1.9×10^8–1.9×10^9 EVs/mL and a limit of detection of 5.9×10^6 EVs/mL. This optimal immunoassay exhibits a 1.92 nM equilibrium dissociation constant for bound EVs, suggesting a high binding affinity when CD81 is targeted. Our study provides important insights into surface chemistry development for EV detection targeted via transmembrane protein biomarkers using antibodies, which has promising applications for disease diagnostics.

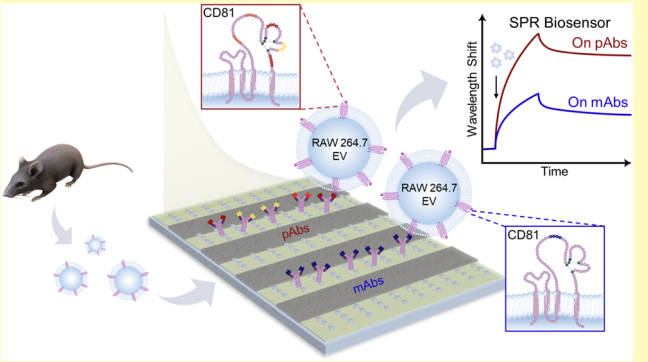

KEYWORDS: *extracellular vesicles, biomarkers, surface plasmon resonance, biosensors, self-assembled monolayer, tetraspanin*

Extracellular vesicles (EVs) are nanometer-sized particles secreted by most cells.[1−4] EVs have a rich presence in liquid biopsy with concentrations in the order of 10^9 EVs/mL in human blood serum.[5−8] Depending on their biogenesis, function, and size, EVs are classified as exosomes, microvesicles, and apoptotic bodies.[9−12] Exosomes are the most abundant EV type with sizes between 30−150 nm,[12−15] carrying proteins inherent from the endosomal region of the parent cells and considered as diagnostic markers.[16] Transmembrane protein (TMP) biomarkers are differentially expressed in morbid cells and the EVs they release,[17−20] providing opportunities for their application in clinical settings. Tetraspanins comprise a large subset of TMPs, playing roles in cellular proliferation, mobility, and activation.[21] Specifically, CD81 is a suitable target for high EV uptake as it is involved in the progression of many diseases,[22−24] and it is widely expressed in most cells.

EV samples differ in size and biological nature compared to protein antigens thereby introducing various levels of complexity for their detection.[8] Current EV-based proteomic characterization immunoassays involve targeting intact or lysed EVs for TMP profiling and molecular cargo analyses.[25] These include fluorescent nanoparticle tracking analysis, ExoView, flow cytometry, Western blot, and enzyme-linked immunosorbent assay (ELISA).[8,26−32] Previous ELISA studies have reported a limit of detection (LOD) of 8.34×10^9 EVs/mL from MCF-7-derived exosomes.[33] Measurements using flow cytometry have reported a LOD of 4.6×10^8 EVs/mL for breast cancer (BT-474) derived EVs.[34] These technologies, however, require fluorescent labeling, are laborious, insufficiently sensitive, and expensive.

Surface plasmon resonance (SPR) biosensors are a powerful tool to study protein−protein interactions because of their direct, real-time, and label-free technology.[35] SPR biosensors

Received: March 8, 2024
Revised: May 8, 2024
Accepted: June 17, 2024

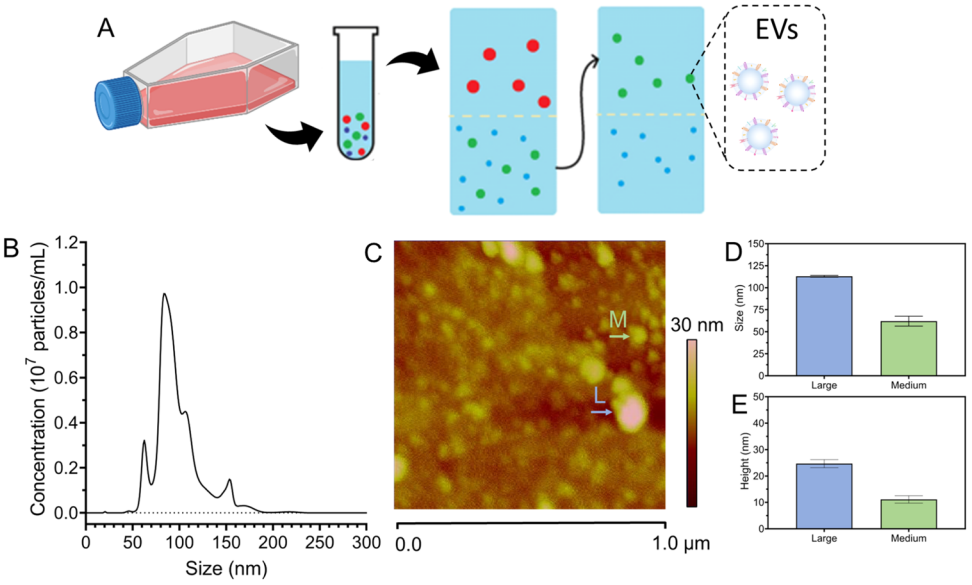

Figure 1. Isolation and Characterization of RAW 264.7 EVs. (A) Schematic representation of the RAW 264.7 EV isolation methodology via ultrafiltration. (B) NTA graph for size and concentration measurements of EVs. (B) AFM topography image showing dry EVs on mica from PBS buffer. (C) Lateral size and (D) height of EVs measured from AFM images.

measure changes in refractive index when a specific biorecognition event (e.g., antibody to antigen) occurs near a noble metal surface (e.g., gold) where a surface plasmon resonance is generated upon impingement of light. They use chemical coatings such as self-assembled monolayers (SAMs) that provide low-fouling backgrounds with functional groups to bind biorecognition elements (BREs) for antigen detection.[36,37] SPR biosensors have numerous applications in biotechnology, medical diagnostics, and drug screening,[27,38] with reported subnanomolar detection of protein concentrations.

SPR biosensors have been extensively applied in the detection of EV samples using antibodies (Abs)[39−52] with focus on the targeting of tetraspanin markers like CD81, CD63, CD9, and disease-specific TMPs. Biotin−avidin chemistries for antibody (Ab) immobilization are most often used, followed by EV detection targeting TMPs. Furthermore, sandwich assays are sometimes implemented to identify EV subpopulations, resulting in excellent biosensor performance with low LOD. For instance, SPR biosensors were applied to detect EVs isolated from breast cancer cell lines using gold chips to immobilize CD9 and CD63 monoclonal Abs via biotin−avidin surface chemistry.[48] Subpopulations of HER-2(+) EVs were determined using a sandwich assay, resulting in a linear range of 2.07×10^6−3.3×10^7 EVs/mL and LOD of 2.07×10^6 EVs/mL. Similarly, HER-2 Abs were oriented onto SPR chips using biotin−streptavidin chemistry to detect EVs in serum from BT474 cells, which resulted in a linear range and LOD of $(0.8–3.31) \times 10^7$ EVs/mL and 8.28×10^6 EVs/mL, respectively.[47] Recently, Kowalczyk et al. used SPR biosensors to detect EVs from human lung cancer cells.[41] Their study reports equilibrium dissociation constants of 4.77 μM, 44.1 nM, and 0.09 nM when EVs were respectively targeted via CD81, CD63, and CD9 using Abs immobilized onto protein A-functionalized SPR chips. Yang et al. reported an equilibrium dissociation constant of ∼0.79 nM for EVs from human lung cancer A549 cell lines interacting with CD63 Abs immobilized via NHS/EDC chemistry onto a layer of 11-Mercaptoundecanoic acid.[46] Notably, most of these works use antibody functionalization strategies with full coverages that do not account for steric hindrance effects. However, great challenges remain in the detection of EVs due to their biological heterogeneousness, size distribution, abundance, the microenvironment and arrangement of the target TMPs, and the EV-sample status (e.g., intact vs lysed EVs). Therefore, it is crucial to conduct systematic studies in order to develop robust bioassays for sensitive and specific detection of EVs using SPR biosensors.

Here, we report on the development of an SPR-based immunoassay for the detection of EVs derived from mouse RAW 264.7 cells targeted via CD81. We conducted a systematic study of the surface chemistry effects on EV detection and binding kinetics. We tuned the ratio of oligo ethylene glycol (OEG) alkanethiolates with the hydroxyl and carboxylic acid terminal groups to control the surface coverage of chemically linked Abs while providing a low-fouling background. We investigated the steric hindrance effects of EV capture by tunning the Ab surface coverages to 80 and 40%. Furthermore, a thorough comparison was made on EV detection using monoclonal (mAb) and polyclonal (pAb) antibodies. With optimal immunoassay conditions, EV concentrations ranging from 4.0×10^7 to 1.9×10^{10} EVs/mL were used to determine kinetic parameters and establish the corresponding detection curve. Using binding kinetics, we determined the relationship between Ab clonality and Ab surface coverage in optimal EV detection, emphasizing steric hindrance effects and epitope recognition properties from Abs. This work provides insights for the development of EV-based biosensing technologies.

RESULTS AND DISCUSSION

Isolation and Characterization of EVs from a Leukemic Mouse Cell Line. We used EVs derived from macrophage leukemic cells (RAW 264.7), which express CD81.[22,53] EVs were isolated from the cell culture medium using ultrafiltration (Figure 1A), then resuspended in

https://doi.org/10.1021/acssensors.4c00558
ACS Sens. XXXX, XXX, XXX−XXX

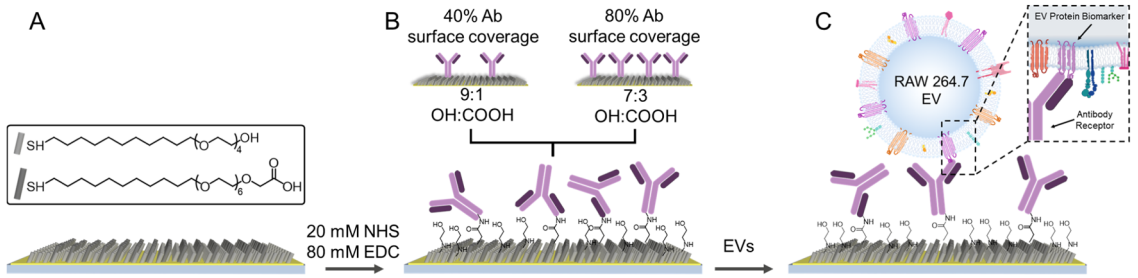

Figure 2. (A) Self-assembled monolayer (SAM) formation with OEG_4OH and OEG_6COOH alkanethiolates. (B) Surface functionalization with CD81 anti-mouse polyclonal or monoclonal Abs via amine coupling NHS/EDC chemistry showing 40 and 80% Ab surface coverages for mixed SAMs with the corresponding 9:1 and 7:3 molar ratios of OEG_4OH/OEG_6COOH. (C) RAW 264.7 EV binding via interactions with CD81 polyclonal or monoclonal Abs and tetraspanin CD81 on EVs.

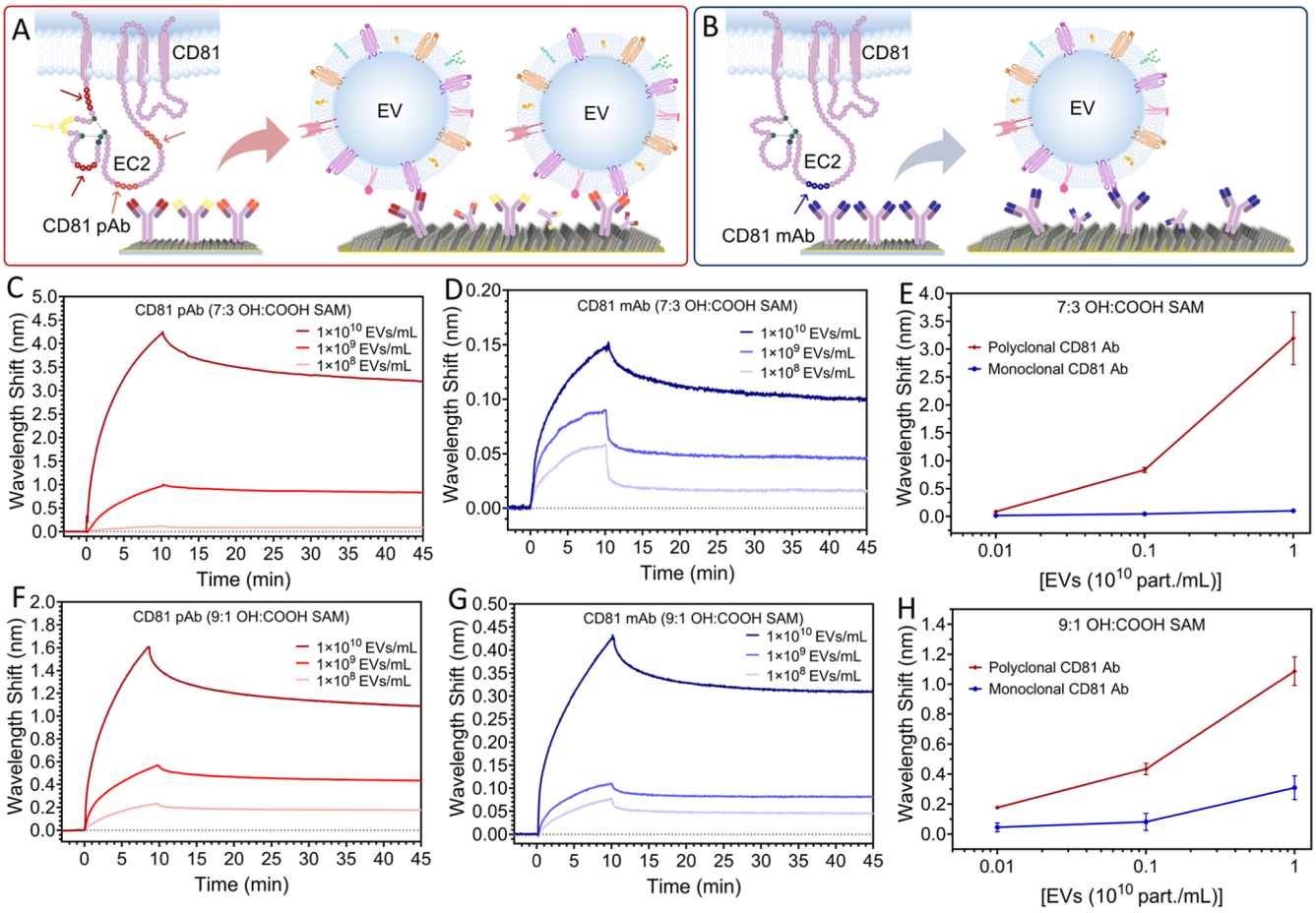

Figure 3. Schematics of one possible binding epitope sequence versus multiple on the EC2 loop of CD81 for (A) CD81 pAb and (B) CD81 mAb, respectively. (C, D) Real-time SPR sensorgram and (E) detection curves of the binding of different concentrations of EVs to CD81 pAb and mAb functionalized surfaces, respectively, on a 7:3 OEG_4OH/OEG_6COOH mixed SAM and 80% antibody surface coverage. (F, G) Real-time SPR sensorgram and (H) detection curves of the binding of different concentrations of EVs to CD81 pAb and CD81 mAb functionalized surfaces, respectively, on a 9:1 OEG_4OH/OEG_6COOH mixed SAM and 40% antibody surface coverage.

phosphate-buffered saline (PBS) with concentrations in the range of 1×10^9–1×10^{10} EVs/mL, and stored in −80 °C for up to 2 weeks. Samples were thawed on ice when needed. NTA measurements show that the sizes of EVs are in the range of 50−180 nm with a mean diameter of 112 nm (Figure 1B), which corresponds to the size of exosomes.[12−15] EV sizes were also measured using atomic force microscopy (AFM). Figure 1C shows heterogeneous size distributions of EVs with mean lateral sizes of 70 and 115 nm for relative medium and large EVs (Figure 1D), respectively, and heights corresponding to 10 and 25 nm. The difference in EV diameter and height is attributed to the spreading of the EV membrane on flat mica and subsequent drying of the dispersion medium (PBS). As a consequence, EV sizes from AFM are smaller compared to NTA measurements.

Surface Functionalization and Immunoassays. The schematics of surface functionalization, Ab immobilization, and EV detection using the SPR biosensor are depicted in Figure 2. Mixed SAMs were formed onto the gold SPR chips with 9:1 and 7:3 molar ratios of OEG_4OH/OEG_6COOH (OH/

https://doi.org/10.1021/acssensors.4c00558
ACS Sens. XXXX, XXX, XXX−XXX

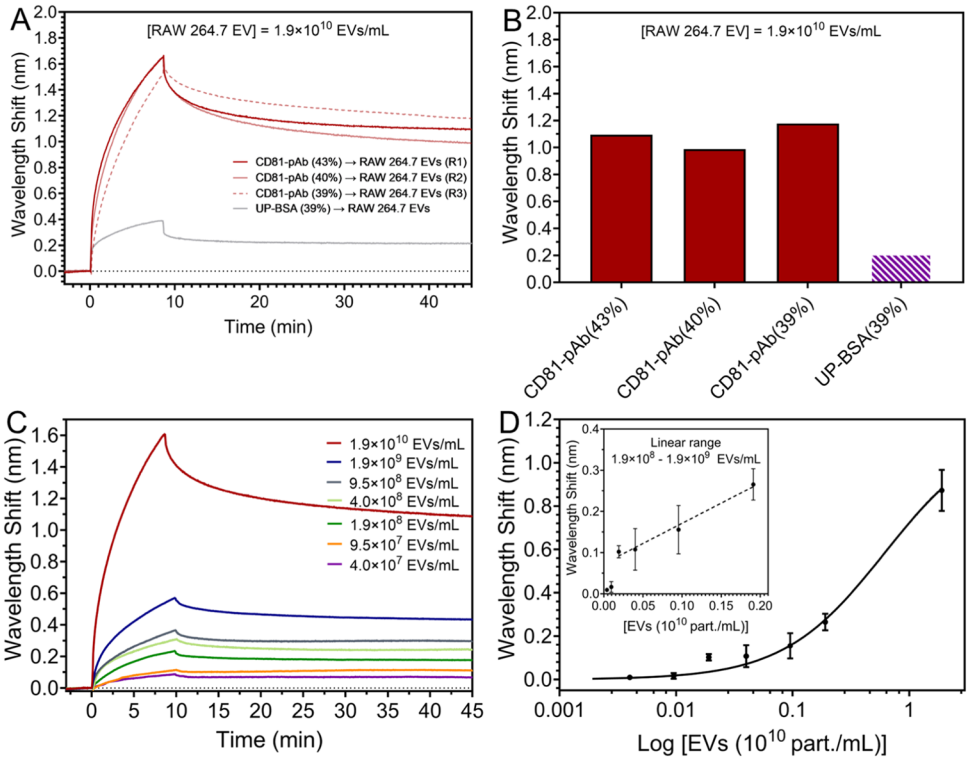

Figure 4. (A) Real-time SPR sensorgrams and (B) wavelength shift of the binding of RAW 264.7 EVs at a concentration of 1.9×10^{10} EVs/mL for three replicates to the sensor surface functionalized with CD81 pAbs and UP-BSA reference on a 9:1 OEG_4OH:OEG_6COOH mixed SAM and 38−43% protein surface coverage. (C) Real-time SPR sensorgram and (D) detection curve, highlighting the linear detection range, of different EVs concentrations between 4.0×10^7−1.9×10^{10} EVs/mL binding to CD81 pAb functionalized surfaces on a 9:1 OEG_4OH/OEG_6COOH mixed SAM and 40% antibody surface coverage.

COOH) alkanethiolates (Figure 2A) to immobilize Abs with 40% (104 ng/cm^2) and 80% (208 ng/cm^2) surface coverage using carbodiimide chemistry[54] while providing a low-fouling background[36] (Figure 2B). The Ab percent surface coverage (θ_{Ab}) estimation is provided in the Supporting Information with Figure S1 showing the antibody dimensions and the estimate of the maximum number of Abs per cm^2. Ultrapure BSA (UP-BSA) was used as a reference channel given its ability to prevent nonspecific binding. A typical sensorgram corresponding to the surface functionalization with CD81 pAbs and UP-BSA solutions is shown in Figure S2. Increasing the OEG_6COOH thiol ratio in SAMs (OH/COOH = 7:3) provides more active sites and larger surface coverages with Abs. Thus, the effect of highly packed Ab surface coverage (θ_{Ab} ∼ 80%) on EV binding can be investigated. The 9:1 SAM mixture with predominantly OEG_4OH terminated groups was chosen to ensure a higher low-fouling background[37,55,56] with enough activated sites for Ab surface coverage (θ_{Ab} ∼ 40%) to reduce the possible steric hindrance on EV binding. As illustrated in Figure 2C, EVs are captured onto the sensor surface via the antibody−tetraspanin interactions when EV samples are flown through the functionalized SPR sensor chip. To evaluate the nonspecific binding of background and UP-BSA functionalized reference surfaces, we collected the SPR sensorgrams of EVs interacting with different control surfaces, including OH-only SAM, deactivated mixed SAMs, BSA, and UP-BSA as well as CD81 pAb functionalized surfaces (Figures S3−S4).

CD81 is one of the ubiquitous EV biomarkers from the tetraspanin family.[57] The structure of tetraspanins contains two extracellular domains comprising one small extracellular loop (EC1) and one large extracellular loop (EC2).[58,59] Polyclonal Abs originate from different B cells in a host animal that can recognize more than one epitope on the same protein[60,61] (Figure 3A). In contrast, mAbs originate from the same B cell in a host animal, and it recognizes only one binding epitope or binding site on a protein[60,62] (Figure 3B). Previous reports suggest that mAbs target the open EC2 loop in CD81.[58] It has been shown that the EC2 loop in CD81 possesses sites that are crucial for recognition and cell interaction whereas the EC1 loop plays a less important role.[63] Furthermore, current therapeutic approaches in developing CD81 Abs have focused on targeting the EC2 loop,[58] and suggesting that Abs bind to the extracellular sites of CD81.[64] We compared mAbs and pAbs in our study to understand the effect of mAbs and pAbs in the binding of the CD81 extracellular sites. Understanding the nature and properties of Abs (such as Ab clonality) is important to select appropriate BREs for EV capturing. While typically avoided in diagnostic settings due to their variability, pAbs could offer a practical solution to the challenges encountered with mAbs in EV detection. Moreover, pAbs are effective in capturing EVs that could be further profiled via sandwich assays.

Detection of EVs via CD81 Abs. CD81 pAbs and mAbs were chemically linked onto a 7:3 OH/COOH SAM with 80% surface coverage. We used EV sample concentrations of 1×10^8, 1×10^9, and 1×10^{10} EVs/mL to assess EV binding. Figure S5 shows the representative sensorgrams of three replicates for the entire surface functionalization and EV detection process as well as the baseline noise and its standard deviation. The AFM images taken from an EV sample flown over a CD81 mAb functionalized chip further confirm the

https://doi.org/10.1021/acssensors.4c00558
ACS Sens. XXXX, XXX, XXX−XXX

capture of EVs onto the SPR sensor surface (Figure S6). The relatively smaller EVs on the sensor surface (Figures S6C,D) indicate that mass diffusion plays an important role in the detection of EVs. Because of the heterogeneity of pAbs, we first tested CD81 pAbs from different companies to assess batch-to-batch variability. The results did not show significant variations across CD81 pAb batches in their ability to capture EVs via CD81 (Figure S7 in the Supporting Information). The SPR sensorgrams of EV detection using CD81 pAbs and mAbs with a coverage of 80% are shown in Figure 3C,D, respectively. For each concentration of EVs, CD81 pAbs bind EVs more effectively than CD81 mAbs. Specifically, the wavelength shifts for EVs captured by CD81 pAbs ranged from 3.19 to 0.08 nm for concentrations of 1×10^{10} EVs/mL down to 1×10^{8} EVs/mL, respectively. For mAbs, these changes ranged from 0.09 to 0.01 nm for the same concentrations. Figure 3E shows the detection curves, further demonstrating the stronger binding of EVs via CD81 pAbs than mAbs.

We also assessed the capture of EVs using CD81 pAbs and mAbs chemically linked onto a 9:1 (OH/COOH) SAM with a 40% surface coverage for the same EV sample concentrations. The SPR sensorgrams in Figure 3F,G show that the wavelength shifts for EVs captured by CD81 pAbs ranged from 1.08 to 0.17 nm, compared to those from 0.30 to 0.04 nm for CD81 mAbs, for concentrations of 1×10^{10} EVs/mL down to 1×10^{8} EVs/mL, respectively. Consistently, CD81 pAbs capture more EVs via CD81 compared to mAbs even for the lower antibody surface coverages. Unlike the 80% surface coverage, the 40% surface coverage CD81 mAbs bind more EVs mainly due to reduced steric hindrance effects. Figure 3H shows the detection curves with 40% antibody surface coverage. The wavelength shifts for CD81 pAbs with 40% surface coverage are lower than those for 80% surface coverage (Figure 3E,H), suggesting that the effect of reduced binding sites on the sensor surface is more pronounced than that of steric hindrance for pAbs. However, the wavelength shifts for CD81 mAbs with 40% surface coverage are higher than those for 80% surface coverage, suggesting the reversed two effects for mAbs. As illustrated in Figure 3B, CD81 mAbs can bind to one epitope on the EC2 loop. The binding sites on CD81 mAbs could not be accessible by the epitope on the EC2 loop of CD81 on EVs when the surface coverage of CD81 mAbs is high. Therefore, a lower CD81 mAb surface coverage could benefit the capture of EVs. In contrast, a less steric hindering effect could affect the capture of EVs by CD81 pAbs because more epitopes on the EC2 loop of CD81 on EVs can be recognized by CD81 pAbs. From these results, a surface coverage of 40% using pAbs immobilized onto a 9:1 OH:COOH SAM was identified as optimal for EV capture using our SPR biosensing platform.

Limit of Detection and Linear Range of EVs Targeted via CD81 pAbs. Using the optimal immunoassay, we estimated the LOD and linear range of EV detection in our system. Figure 4A shows the SPR sensorgrams of three experimental replicates for the detection of EVs at a concentration of 1.9×10^{10} EVs/mL and the corresponding reference channel that immobilized UP-BSA with a similar surface coverage. It is worth noting that each replicate was performed with different SPR chips and EVs isolated from various cell culture batches. Thus, the results demonstrate that the immunoassays are robust and the detection of EVs is highly reproducible, which also indicates that the protocols for EV sample preparation are highly reproducible. The wavelength shifts of each replicate and the reference channel are plotted in Figure 4B. The average wavelength shift was 1.08 ± 0.09 nm for the detection of EVs at the concentration of 1.9×10^{10} EVs/mL prior to subtraction with the reference channel. The reference channel showed a wavelength shift of 0.21 nm. The SPR sensorgrams and wavelength shifts for individual measurements of 7 concentrations in the range of 4.0×10^{7}−1.9×10^{9} EVs/mL with their corresponding reference channels are shown in Figures S8−S13. Figure 4C shows the representative sensorgrams for the detection of all EV samples with concentrations from 4.0×10^{7}−1.9×10^{10} EVs/mL. The detection curve is shown in Figure 4D, and a linear detection is in the range of 1.9×10^{8}−1.9×10^{9} EVs/mL (Figure 4D inset). Compared to previous reports,[47,48] our linear range spans EV concentrations 1 order of magnitude higher. The LOD was estimated according to $3\sigma/S$, where σ is the standard deviation of the blank signal (Figure S5), and S is the slope of the calibration curve. The LOD of our EV detection was estimated to be 5.9×10^{6} EVs/mL, which is about 2 orders of magnitude larger than a recently reported value.[41] Even though CD81 on the EV surface was used as a target tetraspanin in the earlier work, the EVs were produced from human lung cancer cells and CD81 mAbs were immobilized on the surface via protein A, which may offer a better antibody orientation to improve the LOD. Compared to other reports,[47,48] our LOD is comparable but with the advantage of omitting sandwich assays. Nonetheless, we demonstrate that our SPR platform can capture EVs in the level of up to 3 orders of magnitude lower than the EV concentration often found in serum.[5−8]

Binding Kinetics of CD81 on EVs with CD81 pAbs and mAbs. The real-time SPR sensorgrams of different EV concentrations allow us to conduct the study of binding kinetics of CD81 on the surface of EVs with CD81 pAbs and mAbs. Understanding binding kinetics of EVs via TMPs is important as these parameters provide fundamental knowledge that is used to identify pathways to inhibit specific binding interactions if they are associated with disease progression.[65] Knowing the binding affinity of CD81 on EVs to Abs, for example, can guide fundamental studies to understand how small molecule interactions with CD81 can be as specific as possible to prevent undesirable side effects. We applied a direct target-ligand binding assay model for the kinetic analysis. This model is described by the interaction between the CD81 pAbs or mAbs and CD81 on the surface of EVs (CD81−EV) to form an EV−pAb (or mAb) complex. Equation 1 shows the interaction between the CD81 pAbs and CD81−EV.

$$[\text{CD81}-\text{pAb}] + [\text{CD81}-\text{EV}] \underset{k_d}{\overset{k_a}{\rightleftharpoons}} [\text{EV}-\text{pAb}] \quad (1)$$

The kinetic parameters such as the association rate k_a, the dissociation rate k_d, and the equilibrium dissociation constant K_D can be estimated from the SPR sensorgrams obtained during the EV binding step. We used the optimal immunoassay to establish the binding kinetics model. A nonlinear global fitting was performed to the SPR sensorgrams obtained with EV concentrations ranging from 4.0×10^{7}−1.9×10^{9} EVs/mL. The high EV concentration of 1.9×10^{10} EVs/mL was not included to avoid bulk surface effects. Similarly, sensorgrams from lower concentrations were picked as they are preferred for estimating binding kinetics more accurately. We used nonlinear global fitting for the association (Figure 5A) and

https://doi.org/10.1021/acssensors.4c00558
ACS Sens. XXXX, XXX, XXX−XXX

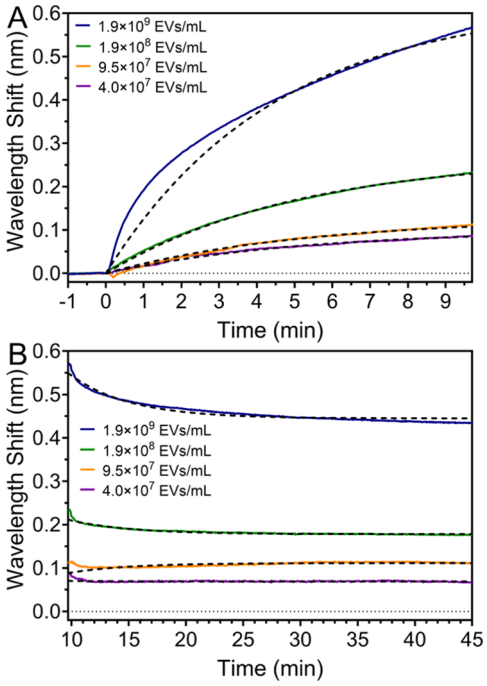

Figure 5. (A) Association and (B) dissociation curves of experimental data (solid lines) versus kinetic fittings (dashed lines) of the binding of RAW 264.7 EVs to the sensor surface functionalized with CD81 pAbs. The sensor surface was immobilized with a 9:1 OEG_4OH/OEG_6COOH mixed SAM and functionalized with CD81 pAbs with a 38−43% surface coverage.

dissociation (Figure 5B) phases of the SPR sensorgrams. The K_D value was obtained as a ratio of the corresponding kinetic parameters (k_d/k_a). It is important to note that the units of K_D are usually reported in the units of nM or M. However, no reported K_D values for EVs in the literature have explained what is meant by EV molarity. In our study, we introduce an EV-CD81-based molarity concentration concept on the basis of total protein concentration measurement estimates, which is presented in the Supporting Information (Figure S14). We report k_a and k_d with values of 1.62×10^6 $M^{-1}\cdot s^{-1}$ and 3.20×10^{-3} s^{-1}, respectively. The K_D value obtained was 1.97 nM indicating a strong binding affinity[66] between EVs to CD81 pAbs.

We further investigated the effects of Ab clonality and Ab surface coverage on EV binding kinetics. We used the same method to fit the sensorgrams of EV binding on the pAbs and mAbs with 40 and 80% surface coverages (Figure 3C,D and F,G). The fitting curves are shown in Figures S15−S16 and the kinetic parameters are summarized in Table 1. The k_a and k_d were in the same order of magnitude when using pAbs at a 40% surface coverage whether with smaller EV concentration ranges (Figure 5) or with EV concentrations 1 order of magnitude higher (Figure S16). Comparable K_D values of 1.97 and 2.12 nM were calculated, respectively, with a stronger binding affinity resulting from fitting lower concentrations. Increasing the pAb surface coverage to 80% resulted in a k_a consistent in the order of magnitude with a value of 1.28×10^6 $M^{-1}\cdot s^{-1}$. A slightly slower k_d was observed as 2.41×10^{-3} s^{-1}, resulting in a lower K_D of 1.88 nM and attributed to higher surface coverage pAbs holding stronger onto CD81. From these results, we observe that steric hindrance has a smaller effect when using pAbs for which higher epitope sequence recognition becomes more prevalent.

Table 1. Kinetic Parameters of Interactions between RAW 264.7 EVs and CD81 Abs[a]

CD81 Ab	OH/COOH	θ_{Ab} (%)	K_{on} ($M^{-1}\cdot s^{-1}$)	K_{off} (s^{-1})	K_D (nM)
pAb*	9:1	40	1.62×10^6	3.20×10^{-3}	1.97
pAb	7:3	80	1.28×10^6	2.41×10^{-3}	1.88
pAb	9:1	40	1.25×10^6	2.66×10^{-3}	2.12
mAb	9:1	40	4.91×10^5	4.18×10^{-3}	8.5
mAb	7:3	80	1.95×10^3	6.58×10^{-3}	3.37×10^3

[a]*Denotes the binding kinetics from the previous section described with lower concentrations.

Using CD81 mAbs at a 40% surface coverage significantly decreases the k_a 1 order of magnitude compared to pAbs as the calculated value is 1.25×10^5 $M^{-1}\cdot s^{-1}$. A slightly faster k_d in the same order of magnitude was observed with a value of 4.18×10^{-3} s^{-1}, resulting in a higher K_D of 8.5 nM. Increasing the surface coverage to 80% with mAbs causes a more dramatic decrease in k_a to a value of 1.95×10^3 $M^{-1}\cdot s^{-1}$ as a result from strong steric hindrance effects. The k_d also increased but remained in the same order of magnitude with a value of 6.58×10^{-3} s^{-1}. As a result, the K_D increased significantly to 3.37×10^3 nM. Optimal EV detection via CD81 using mAbs is affected by steric hindrance effects and lower epitope sequence recognition. Comparing mAbs and pAbs at the same surface coverages, we note that the k_a value decreases for mAbs. Furthermore, a higher mAbs surface coverage of 80% will have a stronger steric hindrance effect compared to the lower 40% surface coverage. In general, the K_D is higher using mAbs compared to pAbs for similar experimental conditions.

The interactions between tetraspanins and antibodies are characterized by similar association and dissociation rates from those reported in the literature.[41] A k_a value of 1.76×10^2 $M^{-1}\cdot s^{-1}$ was reported using protein-A sensor chips functionalized with CD81 mAbs to target EVs derived from a human alveolar basal epithelial cell line A549.[41] We report k_as one to 3 orders of magnitude higher using mAbs with values of 1.95×10^3 and 4.91×10^5 for 80 and 40% surface coverages, respectively. Slower association kinetics were explained from processes such as structural arrangements and desolvation.[41] However, the binding of CD81 on EVs to mAbs at lower surface area coverages decreases steric hindrance effects, which is a highly likely reason for the faster association kinetic rates observed from our experiments in comparison. This highlights an advantage of our bioassay to capture EVs via CD81 using well-controlled OEG-SAM surfaces and mAb immobilization at an optimal surface coverage. Notably, faster k_a values ranging from 1.25×10^6−1.62×10^6 $M^{-1}\cdot s^{-1}$ are calculated using CD81 pAbs, which are 4 orders of magnitude higher than previous reports. The effect of pAbs targeting more epitope sequences in the CD81 EC2 loop is attributed to the dramatic increase in k_a values compared to mAbs. The increase in EV capture using biosensing surfaces with optimal chemistry is imperative to further develop techniques focused on EV subpopulation studies for the profiling of diagnostic markers.

CONCLUSIONS

In this work, we develop immunoassays for optimal EV detection using SPR biosensors. Specifically, we studied the effects of Ab clonality and Ab surface coverage, with the associated OEG-SAM ratios for Ab immobilization, on the

https://doi.org/10.1021/acssensors.4c00558
ACS Sens. XXXX, XXX, XXX−XXX

detection of mouse monocyte RAW 264.7 EVs. We obtained the limit of detection, linear range, and binding kinetic parameters for the detection of mouse monocyte RAW 264.7 EVs targeted via CD81. We determined that CD81 pAbs immobilized at a 40% surface coverage onto a 9:1 EG_4OH/EG_6COOH SAM are optimal for EV capture due to reduced steric hindrance effects and multiple epitope sequences targeted on CD81. Our limit of detection is comparable to other reported values from the literature, which is at least 3 orders of magnitude lower than the typical concentration of EVs in serum. The linear range reported in this work spans higher EV concentrations compared to other values in the literature, which could be advantageous when clinical samples with higher EV concentrations are needed. Our reported equilibrium dissociation constants using CD81 pAbs show a strong binding affinity to CD81 on EVs. We established that when using pAbs, varying the surface coverage has little effect on the resulting kinetic parameters as a broader Ab epitope sequence recognition property is more prominent compared to steric hindrance from higher Ab packing. The equilibrium dissociation constants for pAbs are lower, showing stronger binding affinities compared to mAbs regardless of Ab surface coverages. Finally, for mAbs, steric hindrance effects resulting from high Ab surface coverage are prominent, decreasing the association rates and overall binding affinity to CD81 on EV surfaces. This study provides fundamental insights into the effect of surface chemistry in immunoassay development using SPR biosensors with important implications that can further the development of EV-based medical diagnostic platforms.

MATERIALS AND METHODS

Chemicals and Reagents. Oligo ethylene glycol (EG) alkanethiolates HS-$(CH_2)_{11}$-$(OC_2H_4)_4$-OH and HS-$(CH_2)_{11}$-$(OC_2H_4)_6$-OCH_2-COOH were purchased from ProChimia Surfaces. *N*-Hydroxysuccinimide, UltraPure BSA, CD81 Monoclonal Antibody, and Pierce 660 nm Protein Assay Reagent were purchased from Thermofisher Scientific. *N*-(3-(Dimethylamino)propyl)-*N*′-ethylcarbodiimide hydrochloride, and Sodium chloride (NaCl) ≥ 99.0% were purchased from Millipore Sigma. CD81 polyclonal antibody was purchased from the Proteintech Group, Inc. RAW 264.7 cells were obtained from the American Type Culture Collection (ATCC). The Dulbecco's modified eagle medium (DMEM) (1X), Opti-MEM reduced serum medium, and Fetal Bovine Serum (FBS) were purchased from Gibco. Phosphate-buffered saline (PBS), 10X concentrate, pH 7.4 molecular biology grade was purchased from Corning, Mediatech, Inc. Ethanolamine hydrochloride ≥98.0% (by trimetric analysis) was purchased from the Tokyo Chemical Industry Co., Ltd. (TCI) America. Sodium acetate, anhydrous, 99% was purchased from BeanTown Chemical, Inc. Hydrogen Peroxide, 30%, BAKER ANALYZED ACS Reagent grade was purchased from J.T. Baker. Sulfuric Acid (Certified ACS Plus) and absolute ethanol 200-proof were purchased from Fisher Scientific. Poly-(tetrafluoroethylene) (PTFE) 0.45 μm filters, 25 mm in diameter were purchased from Cole-Parmer. Ultra centrifugal filters, 100 kDa MWCO were purchased from Amicon. A silicon cantilever (NSG30) with a force constant of 22−100 $N{\cdot}m^{-1}$ and resonant frequency of 240−440 kHz for tapping-mode atomic force microscopic (TM-AFM) measurements was obtained from Bruker AFM Probes.

Cell Culture and Isolation of EVs. RAW 264.7 cell line was maintained in T25 flasks, incubated at 37 °C, and 5% CO_2 in the presence of 5 mL of DMEM with 10% FBS. Media changes were performed every other day to maintain nutrient levels, washing the cell culture flask with ∼3 mL of prewarmed fresh medium twice before full medium substitution. Cell passage was performed after 70−80% confluency was reached. Once the primary cell culture was established, we transferred 2.1 million cells to T75 culture flasks for EV production and harvest. The cell culture medium was replaced with 15 mL of Opti-MEM reduced serum medium, with the flask washed with 5 mL of prewarmed Opti-MEM. Under this condition, EVs were produced for a duration of up to 3 days at 37 °C. The cell culture medium was then collected for EV isolation. The debris and detached cells were eliminated by centrifuging at 300*g* for 10 min, with larger vesicles removed by filtering the supernatant through 0.45 μm PTFE filters. Then, we centrifuged the collected media at 3000*g* for 5−10 min at 4 °C using the ultrafiltration tubes until a death volume of about 200 μL was reached. The retentate containing the EVs was washed by resuspension with PBS and centrifuged at 3000*g* for 5−10 min at 4 °C until a death volume of 200 μL was reached again. The washing process was repeated five times. The resulting retentate containing EVs was collected, diluted 1:10 in PBS, and distributed in 100−200 μL aliquots. All EV aliquots were stored at −80 °C for up to 2 weeks.

Nanoparticle Tracking Analysis. We analyzed the mean diameter and concentration of EVs using a NanoSight NS300 (Malvern Panalytical Ltd., U.K.) equipped with a 488 nm blue laser. For each measurement, we captured five 60 s videos and analyzed them using the built-in NanoSight software NTA 3.2. Before each measurement, each EV sample was thawed on ice from −80 °C storage and diluted 1:200 in PBS.

Total Protein Assay. We used the Thermofisher Scientific Pierce 660 nm Protein Assay kit. Briefly, 10 μL of freshly thawed EVs was mixed with 150 μL of the protein assay reagent onto a 96-well plate with an optical clear bottom and a black wall. A negative control with 150 μL of the protein assay reagent with 10 μL PBS was also added. The plate was covered and mixed on a plate shaker for 1 min, incubating for 5 min at room temperature. The absorbance of the unknown sample was measured at 660 nm. The reading was compared with a pre-established BSA calibration curve to determine the final total protein concentration of the EV sample in μg/mL.

Atomic Force Microscopy. The morphology, diameter, and height of EVs were characterized with TM-AFM using a Digital Multimode AFM equipped with a Nanoscope IVa controller. A silicon cantilever (NSG30) was used for the measurements. Each measurement was obtained at a scan rate of 1.00 Hz in a 512 × 512-point frame. Each sample was prepared by pipetting 20 μL of freshly thawed (on ice from −80 °C storage) undiluted EV samples onto a 7 × 7 mm of an atomically flat mica sheet and allowed to dry at room temperature. For the samples characterized after the SPR experiments, the gold chips containing captured EVs were carefully cut onto squares of 7 × 7 mm and imaged immediately after the sample was dried out from water flow. The lateral size and height of EVs were measured from AFM images using the built-in software.

SPR Biosensor. A laboratory SPR biosensor developed at the Institute of Photonics and Electronics, Prague, Czech Republic, was used in this study.[67] The 6-channel SPR biosensor with temperature stabilization is based on the wavelength spectroscopy of surface plasmons. The instrument consists of a dispersionless microfluidic system, which allows for the delivery of the sample analyte directly to the surface of the SPR chip, using a two-pump system, without the effects of inter- and intra-dispersion. The incident light is collimated and polarized in the sensor head prior to its introduction to the SPR coupling prism. The reflected light is then collected and coupled to a 6-channel spectrograph. The SPR gold chips were prepared by coating conventional glass slides with a thin layer of titanium (1−2 nm) and gold (48 nm) via electron-beam evaporation at the Cornell NanoScale Facility (CNF). The SPR chip is then interfaced with the coupling prism using immersion oil that matches the refractive index of the prism, preventing any irrelevant signals from the prism coupling. A flow cell with six separate flow chambers facing each sensing spot is interfaced with the chip to confine the sample during the experiment. Each flow cell is about 80 μm in depth. The liquid sample is delivered onto the flow cell and sensor surface using a peristaltic pump. The sensor is equipped with a temperature controller (ILX Lightwave, LDT-5525) to maintain accurate control in the range of 5−40 °C. For the SPR sensor used in this study, a 1 nm SPR wavelength shift corresponds to a change in the protein surface coverage of 17 ng/

https://doi.org/10.1021/acssensors.4c00558
ACS Sens. XXXX, XXX, XXX−XXX

cm^2.[68] This correlation is then used to calibrate the change in the surface coverage of bound antibodies.

Surface Functionalization and Antibody Immobilization. Gold-coated SPR chips were washed with a 3:1 H_2SO_4/H_2O_2 piranha mixture for 5 min to remove organic impurities on the surface. The chips were then rinsed with 18.2 MΩ·cm Milli-Q water and ethanol and dried with nitrogen. The gold surface was further subject to oxygen plasma cleaner at "Medium" RF power on a Harrick Plasma Cleaner (115 V, 30 W max. RF) for 5 min. It was then rinsed with Milli-Q water and ethanol and dried with nitrogen. The SPR chips were then immersed in 0.2 mM ethanol solutions of OEG_4OH and OEG_6COOH thiols in molar ratios of 9:1 and 7:3 OEG_4OH/OEG_6COOH, respectively, for 12−16 h. The SPR chips were removed from the ethanolic thiol solutions, rinsed with ethanol and Milli-Q water and dried with nitrogen. The chip was mounted onto the SPR sensor attaching the glass side to the prism using immersion oil that matches the refractive index of the prism. All SPR experiments were conducted at a fixed temperature of 25 °C with a baseline stability of 0.01 °C. The Ab immobilization was conducted in real time. Briefly, a baseline was established under Milli-Q water at a flow rate of 20 μL/min. Then, the carboxylate groups from the OEG_6COOH thiols were activated with a preprepared mixture of NHS (20 mM) and EDC (80 mM) in Milli-Q water for 10 min at a flow rate of 5 μL/min followed by Milli-Q wash at 20 μL/min. Sodium acetate buffer (10 mM) (SA-10), pH 5.0 was then introduced. The mAb and pAb solutions with concentrations between 3.5 μg/mL to 7.5 μg/mL in SA-10, pH 5.0 were injected for 15 min at 20 μL/min, aiming for 38−43% and 77−81% Ab surface coverage as needed. The calculation of antibody surface coverage is provided in the Supporting Information with Figure S1 showing the theoretical estimate for the total number of bound Abs per cm^2 based on Ab molecular dimensions. Analogously, a solution of 500 μg/mL UP-BSA was exposed for the same time length to functionalize the reference channels. The functionalized surface was washed with SA-10 for 3 min, followed by a 2 min exposure with high ionic strength PBS 0.5 M NaCl (PBS-Na), to remove all noncovalently, loosely bound ligands. A short wash with SA-10 followed. The residual unreacted NHS groups were deactivated by injecting an ethanolamine buffer solution 1 M, pH 8.0 for 10 min at 20 μL/min. SA-10 buffer was injected again to establish the final Ab immobilization levels.

Detection of RAW 264.7 EVs Bound to CD81 Abs. PBS buffer (pH 7.4) was used for the detection phase. EV samples were flown over the Ab-functionalized and reference surfaces (UP-BSA immobilized) for 10 min at 30 μL/min. Three experimental replicates were performed for all CD81 Ab-EV experiments. The concentrations used were 4.0×10^7, 9.5×10^7, 1×10^8, 1.9×10^8, 4.0×10^8, 9.5×10^8, 1×10^9, 1.9×10^9, 1×10^{10}, and 1.9×10^{10} EVs/mL. Exposure with PBS buffer followed postdetection at the standard flow rate of 20 μL/min, the same that was used to establish the baseline. For binding kinetic calculations, PBS buffer was flown for at least 35 min post sample detection. The final detection levels of EVs bound to CD81 Abs were assessed as the difference in the wavelength shift between the buffer baselines before sample injection and after PBS washing.

■ ASSOCIATED CONTENT

Supporting Information

The Supporting Information is available free of charge at https://pubs.acs.org/doi/10.1021/acssensors.4c00558

Antibody surface coverage estimation; a full representative SPR sensorgram, showing the three replicates for the entire surface functionalization and EV detection process, including the baseline noise and its standard deviation; SPR sensorgrams of EV interacting with different control surfaces that include OH-only SAM, deactivated mixed SAM, BSA, and UP-BSA; SPR Sensorgrams for immobilization of CD81 pAbs and UP-BSA; real-time SPR sensorgrams and unsubtracted wavelength shift of the binding of EVs at concentrations ranging from 4.0×10^7−1.9×10^9 EVs/mL; total protein assay schematic with BSA calibration curve used to determine the total protein concentration of EVs; and association and dissociation curves of experimental data vs kinetic fitting of the binding of EVs to the sensor surface functionalized with CD81 mAbs and pAbs immobilized at 40 and 80% surface coverages, respectively (PDF)

■ AUTHOR INFORMATION

Corresponding Author

Qiuming Yu − *Robert Frederick Smith School of Chemical and Biomolecular Engineering, Cornell University, Ithaca, New York 14853, United States;* orcid.org/0000-0002-2401-4664; Email: qy10@cornell.edu

Authors

Jesus M. Lopez Baltazar − *Robert Frederick Smith School of Chemical and Biomolecular Engineering, Cornell University, Ithaca, New York 14853, United States;* orcid.org/0009-0004-7704-093X

Wenchao Gu − *Meinig School of Biomedical Engineering, Cornell University, Ithaca, New York 14853, United States;* orcid.org/0000-0002-0967-1682

Markéta Bocková − *Robert Frederick Smith School of Chemical and Biomolecular Engineering, Cornell University, Ithaca, New York 14853, United States; Institute of Photonics and Electronics, Prague 182 51, Czech Republic*

Complete contact information is available at: https://pubs.acs.org/10.1021/acssensors.4c00558

Notes

The authors declare no competing financial interest.

■ ACKNOWLEDGMENTS

The authors gratefully acknowledge the financial support from the National Science Foundation (NSF) (CBET-2247222). J.M.L.B. acknowledges the support from the National GEM Consortium Fellowship. This work was performed in part at the Cornell NanoScale Facility, a member of the National Nanotechnology Coordinated Infrastructure (NNCI), which is supported by the NSF (Grant NNCI-2025233). Any opinions, findings, conclusions, or recommendations expressed in this material are those of the authors and do not necessarily reflect the views of the NSF.

■ REFERENCES

(1) Couch, Y.; Buzàs, E. I.; Di Vizio, D.; Gho, Y. S.; Harrison, P.; Hill, A. F.; Lötvall, J.; Raposo, G.; Stahl, P. D.; Théry, C.; et al. A brief history of nearly EV-erything - The rise and rise of extracellular vesicles. *J. Extracell. Vesicles* **2021**, *10* (14), No. e12144.

(2) Doyle, L. M.; Wang, M. Z. Overview of Extracellular Vesicles, Their Origin, Composition, Purpose, and Methods for Exosome Isolation and Analysis. *Cells* **2019**, *8* (7), 727.

(3) EL Andaloussi, S.; Mäger, I.; Breakefield, X. O.; Wood, M. J. Extracellular vesicles: biology and emerging therapeutic opportunities. *Nat. Rev. Drug Discovery* **2013**, *12* (5), 347−357.

(4) Liao, Z.; Liu, H.; Ma, L.; Lei, J.; Tong, B.; Li, G.; Ke, W.; Wang, K.; Feng, X.; Hua, W.; et al. Engineering Extracellular Vesicles Restore the Impaired Cellular Uptake and Attenuate Intervertebral Disc Degeneration. *ACS Nano* **2021**, *15* (9), 14709−14724.

(5) Fais, S.; O'Driscoll, L.; Borras, F. E.; Buzas, E.; Camussi, G.; Cappello, F.; Carvalho, J.; Cordeiro da Silva, A.; Del Portillo, H.; El Andaloussi, S.; et al. Evidence-Based Clinical Use of Nanoscale

Extracellular Vesicles in Nanomedicine. *ACS Nano* **2016**, *10* (4), 3886−3899.
(6) Armstrong, J. P. K.; Holme, M. N.; Stevens, M. M. Re-Engineering Extracellular Vesicles as Smart Nanoscale Therapeutics. *ACS Nano* **2017**, *11* (1), 69−83.
(7) Johnsen, K. B.; Gudbergsson, J. M.; Andresen, T. L.; Simonsen, J. B. What is the blood concentration of extracellular vesicles? Implications for the use of extracellular vesicles as blood-borne biomarkers of cancer. *Biochim. Biophys. Acta, Rev. Cancer* **2019**, *1871* (1), 109−116.
(8) Lim, C. Z. J.; Zhang, L.; Zhang, Y.; Sundah, N. R.; Shao, H. New Sensors for Extracellular Vesicles: Insights on Constituent and Associated Biomarkers. *ACS Sens.* **2020**, *5* (1), 4−12.
(9) Jiang, J.; Huang, Y.; Zeng, Z.; Zhao, C. Harnessing Engineered Immune Cells and Bacteria as Drug Carriers for Cancer Immunotherapy. *ACS Nano* **2023**, *17* (2), 843−884.
(10) Huang, C.; Zhou, Y.; Feng, X.; Wang, J.; Li, Y.; Yao, X. Delivery of Engineered Primary Tumor-Derived Exosomes Effectively Suppressed the Colorectal Cancer Chemoresistance and Liver Metastasis. *ACS Nano* **2023**, *17* (11), 10313−10326.
(11) Woo, H.-K.; Sunkara, V.; Park, J.; Kim, T.-H.; Han, J.-R.; Kim, C.-J.; Choi, H.-I.; Kim, Y.-K.; Cho, Y.-K. Exodisc for Rapid, Size-Selective, and Efficient Isolation and Analysis of Nanoscale Extracellular Vesicles from Biological Samples. *ACS Nano* **2017**, *11* (2), 1360−1370.
(12) Tenchov, R.; Sasso, J. M.; Wang, X.; Liaw, W.-S.; Chen, C.-A.; Zhou, Q. A. Exosomes—Nature's Lipid Nanoparticles, a Rising Star in Drug Delivery and Diagnostics. *ACS Nano* **2022**, *16* (11), 17802−17846.
(13) Richardson, J. J.; Ejima, H. Surface Engineering of Extracellular Vesicles through Chemical and Biological Strategies. *Chem. Mater.* **2019**, *31* (7), 2191−2201.
(14) Hassanpour Tamrin, S.; Sanati Nezhad, A.; Sen, A. Label-Free Isolation of Exosomes Using Microfluidic Technologies. *ACS Nano* **2021**, *15* (11), 17047−17079.
(15) Ibsen, S. D.; Wright, J.; Lewis, J. M.; Kim, S.; Ko, S.-Y.; Ong, J.; Manouchehri, S.; Vyas, A.; Akers, J.; Chen, C. C.; et al. Rapid Isolation and Detection of Exosomes and Associated Biomarkers from Plasma. *ACS Nano* **2017**, *11* (7), 6641−6651.
(16) Ko, J.; Wang, Y.; Sheng, K.; Weitz, D. A.; Weissleder, R. Sequencing-Based Protein Analysis of Single Extracellular Vesicles. *ACS Nano* **2021**, *15* (3), 5631−5638.
(17) Koteluk, O.; Bielicka, A.; Lemańska, Ż.; Jóźwiak, K.; Klawiter, W.; Mackiewicz, A.; Kazimierczak, U.; Kolenda, T. The landscape of transmembrane protein family members in head and neck cancers: Their biological role and diagnostic utility. *Cancers* **2021**, *13* (19), 4737.
(18) Li, L.; Li, J. Dimerization of Transmembrane Proteins in Cancer Immunotherapy. *Membranes* **2023**, *13* (4), 393.
(19) Marx, S.; Dal Maso, T.; Chen, J.-W.; Bury, M.; Wouters, J.; Michiels, C.; Le Calvé, B. Transmembrane (TMEM) protein family members: Poorly characterized even if essential for the metastatic process. In *Seminars in Cancer Biology*; Elsevier, 2020; Vol. *60*,, pp 96−106.
(20) Schmit, K.; Michiels, C. TMEM proteins in cancer: a review. *Front. Pharmacol.* **2018**, *9*, 1345.
(21) Zhou, Z.; Yang, Z.; Zhou, L.; Yang, M.; He, S. The versatile roles of testrapanins in cancer from intracellular signaling to cell−cell communication: cell membrane proteins without ligands. *Cell Biosci.* **2023**, *13* (1), No. 59.
(22) Mordica, W. J.; Woods, K. M.; Clem, R. J.; Passarelli, A. L.; Chapes, S. K. Macrophage cell lines use CD81 in cell growth regulation. *In Vitro Cell. Dev. Biol. Anim.* **2009**, *45* (5−6), 213−225.
(23) Li, L.; Zhang, F.; Zhang, J.; Shi, X.; Wu, H.; Chao, X.; Ma, S.; Lang, J.; Wu, M.; Zhang, D.; Liang, Z. Identifying Serum Small Extracellular Vesicle MicroRNA as a Noninvasive Diagnostic and Prognostic Biomarker for Ovarian Cancer. *ACS Nano* **2023**, *17* (19), 19197−19210.
(24) Lee, K.; Fraser, K.; Ghaddar, B.; Yang, K.; Kim, E.; Balaj, L.; Chiocca, E. A.; Breakefield, X. O.; Lee, H.; Weissleder, R. Multiplexed Profiling of Single Extracellular Vesicles. *ACS Nano* **2018**, *12* (1), 494−503.
(25) Jiang, C.; Fu, Y.; Liu, G.; Shu, B.; Davis, J.; Tofaris, G. K. Multiplexed Profiling of Extracellular Vesicles for Biomarker Development. *Nano-Micro Lett.* **2021**, *14* (1), No. 3.
(26) Azzouz, A.; Hejji, L.; Kim, K. H.; Kukkar, D.; Souhail, B.; Bhardwaj, N.; Brown, R. J. C.; Zhang, W. Advances in surface plasmon resonance-based biosensor technologies for cancer biomarker detection. *Biosens. Bioelectron.* **2022**, *197*, No. 113767.
(27) Homola, J. Present and future of surface plasmon resonance biosensors. *Anal. Bioanal. Chem.* **2003**, *377* (3), 528−539.
(28) Homola, J. *Surface Plasmon Resonance Based Biosensors*; Springer, 2006.
(29) Bari, S. M. I.; Hossain, F. B.; Nestorova, G. G. Advances in Biosensors Technology for Detection and Characterization of Extracellular Vesicles. *Sensors* **2021**, *21* (22), 7645.
(30) Qian, F.; Huang, Z.; Zhong, H.; Lei, Q.; Ai, Y.; Xie, Z.; Zhang, T.; Jiang, B.; Zhu, W.; Sheng, Y.; et al. Analysis and Biomedical Applications of Functional Cargo in Extracellular Vesicles. *ACS Nano* **2022**, *16* (12), 19980−20001.
(31) Nicoliche, C. Y. N.; de Oliveira, R. A. G.; da Silva, G. S.; Ferreira, L. F.; Rodrigues, I. L.; Faria, R. C.; Fazzio, A.; Carrilho, E.; de Pontes, L. G.; Schleder, G. R.; Lima, R. S. Converging Multidimensional Sensor and Machine Learning Toward High-Throughput and Biorecognition Element-Free Multidetermination of Extracellular Vesicle Biomarkers. *ACS Sens.* **2020**, *5* (7), 1864−1871.
(32) Price, J. M. J.; Hisada, Y.; Hazeldine, J.; Bae-Jump, V.; Luther, T.; Mackman, N.; Harrison, P. Detection of tissue factor−positive extracellular vesicles using the ExoView R100 system. *Res. Pract. Thromb. Haemostasis* **2023**, *7* (4), No. 100177.
(33) Kilic, T.; Valinhas, A. T. D. S.; Wall, I.; Renaud, P.; Carrara, S. Label-free detection of hypoxia-induced extracellular vesicle secretion from MCF-7 cells. *Sci. Rep.* **2018**, *8* (1), No. 9402.
(34) Tang, Q.; Xiao, X.; Li, R.; He, H.; Li, S.; Ma, C. Recent Advances in Detection for Breast-Cancer-Derived Exosomes. *Molecules* **2022**, *27* (19), 6673.
(35) Homola, J. Surface Plasmon Resonance Sensors for Detection of Chemical and Biological Species. *Chem. Rev.* **2008**, *108* (2), 462−493.
(36) Li, L.; Chen, S.; Zheng, J.; Ratner, B. D.; Jiang, S. Protein Adsorption on Oligo(ethylene glycol)-Terminated Alkanethiolate Self-Assembled Monolayers: The Molecular Basis for Nonfouling Behavior. *J. Phys. Chem. B* **2005**, *109* (7), 2934−2941.
(37) Zheng, J.; Li, L.; Tsao, H. K.; Sheng, Y. J.; Chen, S.; Jiang, S. Strong repulsive forces between protein and oligo (ethylene glycol) self-assembled monolayers: a molecular simulation study. *Biophys. J.* **2005**, *89* (1), 158−166.
(38) Masson, J. F. Surface Plasmon Resonance Clinical Biosensors for Medical Diagnostics. *ACS Sens* **2017**, *2* (1), 16−30.
(39) Chin, L. K.; Son, T.; Hong, J.-S.; Liu, A.-Q.; Skog, J.; Castro, C. M.; Weissleder, R.; Lee, H.; Im, H. Plasmonic Sensors for Extracellular Vesicle Analysis: From Scientific Development to Translational Research. *ACS Nano* **2020**, *14* (11), 14528−14548.
(40) Wang, X.; Phan, M. M.; Sun, Y.; Koerber, J. T.; Ho, H.; Chen, Y.; Yang, J. Development of an SPR-based binding assay for characterization of anti-CD20 antibodies to CD20 expressed on extracellular vesicles. *Anal. Biochem.* **2022**, *646*, No. 114635.
(41) Kowalczyk, A.; Gajda-Walczak, A.; Ruzycka-Ayoush, M.; Targonska, A.; Mosieniak, G.; Glogowski, M.; Szumera-Cieckiewicz, A.; Prochorec-Sobieszek, M.; Bamburowicz-Klimkowska, M.; Nowicka, A. M.; Grudzinski, I. P. Parallel SPR and QCM-D Quantitative Analysis of CD9, CD63, and CD81 Tetraspanins: A Simple and Sensitive Way to Determine the Concentration of Extracellular Vesicles Isolated from Human Lung Cancer Cells. *Anal. Chem.* **2023**, *95* (25), 9520−9530.

https://doi.org/10.1021/acssensors.4c00558
ACS Sens. XXXX, XXX, XXX−XXX

(42) Mazouzi, Y.; Sallem, F.; Farina, F.; Loiseau, A.; Tartaglia, N. R.; Fontaine, M.; Parikh, A.; Salmain, M.; Neri, C.; Boujday, S. Biosensing Extracellular Vesicle Subpopulations in Neurodegenerative Disease Conditions. *ACS Sens.* **2022**, *7* (6), 1657−1665.
(43) Picciolini, S.; Gualerzi, A.; Vanna, R.; Sguassero, A.; Gramatica, F.; Bedoni, M.; Masserini, M.; Morasso, C. Detection and Characterization of Different Brain-Derived Subpopulations of Plasma Exosomes by Surface Plasmon Resonance Imaging. *Anal. Chem.* **2018**, *90* (15), 8873−8880.
(44) Grasso, L.; Wyss, R.; Weidenauer, L.; Thampi, A.; Demurtas, D.; Prudent, M.; Lion, N.; Vogel, H. Molecular screening of cancer-derived exosomes by surface plasmon resonance spectroscopy. *Anal. Bioanal. Chem.* **2015**, *407* (18), 5425−5432.
(45) Liu, C.; Zeng, X.; An, Z.; Yang, Y.; Eisenbaum, M.; Gu, X.; Jornet, J. M.; Dy, G. K.; Reid, M. E.; Gan, Q.; Wu, Y. Sensitive Detection of Exosomal Proteins via a Compact Surface Plasmon Resonance Biosensor for Cancer Diagnosis. *ACS Sens.* **2018**, *3* (8), 1471−1479.
(46) Yang, Y.; Zhai, C.; Zeng, Q.; Khan, A. L.; Yu, H. Multifunctional Detection of Extracellular Vesicles with Surface Plasmon Resonance Microscopy. *Anal. Chem.* **2020**, *92* (7), 4884−4890.
(47) Sina, A. A. I.; Vaidyanathan, R.; Wuethrich, A.; Carrascosa, L. G.; Trau, M. Label-free detection of exosomes using a surface plasmon resonance biosensor. *Anal. Bioanal. Chem.* **2019**, *411* (7), 1311−1318.
(48) Sina, A. A. I.; Vaidyanathan, R.; Dey, S.; Carrascosa, L. G.; Shiddiky, M. J.; Trau, M. Real time and label free profiling of clinically relevant exosomes. *Sci. Rep.* **2016**, *6*, No. 30460.
(49) Reiner, A. T.; Ferrer, N.-G.; Venugopalan, P.; Lai, R. C.; Lim, S. K.; Dostálek, J. Magnetic nanoparticle-enhanced surface plasmon resonance biosensor for extracellular vesicle analysis. *Analyst* **2017**, *142* (20), 3913−3921.
(50) Thakur, A.; Qiu, G.; Ng, S.-P.; Guan, J.; Yue, J.; Lee, Y.; Wu, C.-M. L. Direct detection of two different tumor-derived extracellular vesicles by SAM-AuNIs LSPR biosensor. *Biosens. Bioelectron.* **2017**, *94*, 400−407.
(51) Hosseinkhani, B.; van den Akker, N.; D'Haen, J.; D'Haen, J.; Gagliardi, M.; Struys, T.; Lambrichts, I.; Waltenberger, J.; Nelissen, I.; Hooyberghs, J.; Molin, D. G. M. Direct detection of nano-scale extracellular vesicles derived from inflammation-triggered endothelial cells using surface plasmon resonance. *Nanomed. Nanotechnol. Biol. Med.* **2017**, *13* (5), 1663−1671.
(52) Rupert, D. L. M.; Lässer, C.; Eldh, M.; Block, S.; Zhdanov, V. P.; Lotvall, J. O.; Bally, M.; Höök, F. Determination of Exosome Concentration in Solution Using Surface Plasmon Resonance Spectroscopy. *Anal. Chem.* **2014**, *86* (12), 5929−5936.
(53) McDonald, M. K.; Tian, Y.; Qureshi, R. A.; Gormley, M.; Ertel, A.; Gao, R.; Aradillas Lopez, E.; Alexander, G. M.; Sacan, A.; Fortina, P.; Ajit, S. K. Functional significance of macrophage-derived exosomes in inflammation and pain. *Pain* **2014**, *155* (8), 1527−1539.
(54) Welch, N. G.; Scoble, J. A.; Muir, B. W.; Pigram, P. J. Orientation and characterization of immobilized antibodies for improved immunoassays (Review). *Biointerphases* **2017**, *12* (2), No. 02D301.
(55) Taylor, A. D.; Yu, Q.; Chen, S.; Homola, J.; Jiang, S. Comparison of *E. coli* O157:H7 preparation methods used for detection with surface plasmon resonance sensor. *Sens. Actuators, B* **2005**, *107* (1), 202−208.
(56) Kamat, V.; Rafique, A. Designing binding kinetic assay on the bio-layer interferometry (BLI) biosensor to characterize antibody-antigen interactions. *Anal. Biochem.* **2017**, *536*, 16−31.
(57) Mishra, S.; Kumar, A.; Kim, S.; Su, Y.; Singh, S.; Sharma, M.; Almousa, S.; Rather, H. A.; Jain, H.; Lee, J.; et al. A Liquid Biopsy-Based Approach to Isolate and Characterize Adipose Tissue-Derived Extracellular Vesicles from Blood. *ACS Nano* **2023**, *17* (11), 10252−10268.
(58) Bailly, C.; Thuru, X. Targeting of Tetraspanin CD81 with Monoclonal Antibodies and Small Molecules to Combat Cancers and Viral Diseases. *Cancers* **2023**, *15* (7), 2186.
(59) Mizenko, R. R.; Brostoff, T.; Rojalin, T.; Koster, H. J.; Swindell, H. S.; Leiserowitz, G. S.; Wang, A.; Carney, R. P. Tetraspanins are unevenly distributed across single extracellular vesicles and bias sensitivity to multiplexed cancer biomarkers. *J. Nanobiotechnol.* **2021**, *19* (1), No. 250.
(60) Leenaars, M.; Hendriksen, C. F. M. Critical Steps in the Production of Polyclonal and Monoclonal Antibodies: Evaluation and Recommendations. *ILAR J.* **2005**, *46* (3), 269−279.
(61) Stills, H. F. Chapter 11 - Polyclonal Antibody Production. In *The Laboratory Rabbit, Guinea Pig, Hamster, and Other Rodents*; Suckow, M. A.; Stevens, K. A.; Wilson, R. P., Eds.; Academic Press, 2012; pp 259−274.
(62) Liu, J. K. The history of monoclonal antibody development - Progress, remaining challenges and future innovations. *Ann. Med. Surg.* **2014**, *3* (4), 113−116.
(63) Titu, S.; Grapa, C. M.; Mocan, T.; Balacescu, O.; Irimie, A. Tetraspanins: Physiology, Colorectal Cancer Development, and Nanomediated Applications. *Cancers* **2021**, *13* (22), 5662.
(64) Zaccari, I.; Catchpole, B. G.; Laurenson, S. X.; Davies, A. G.; Wälti, C. Improving the Dielectric Properties of Ethylene-Glycol Alkanethiol Self-Assembled Monolayers. *Langmuir* **2014**, *30* (5), 1321−1326.
(65) Hoare, S. R. J.; Fleck, B. A.; Williams, J. P.; Grigoriadis, D. E. The importance of target binding kinetics for measuring target binding affinity in drug discovery: a case study from a CRF1 receptor antagonist program. *Drug Discovery Today* **2020**, *25* (1), 7−14.
(66) Kamat, V.; Rafique, A.; Huang, T.; Olsen, O.; Olson, W. The impact of different human IgG capture molecules on the kinetics analysis of antibody-antigen interaction. *Anal. Biochem.* **2020**, *593*, No. 113580.
(67) Vaisocherová, H.; Sipova, H.; Visova, I.; Bockova, M.; Springer, T.; Ermini, M. L.; Song, X.; Krejcik, Z.; Chrastinova, L.; Pastva, O.; et al. Rapid and sensitive detection of multiple microRNAs in cell lysate by low-fouling surface plasmon resonance biosensor. *Biosens. Bioelectron.* **2015**, *70*, 226−231.
(68) Vaisocherová, H.; Zhang, Z.; Yang, W.; Cao, Z.; Cheng, G.; Taylor, A. D.; Piliarik, M.; Homola, J.; Jiang, S. Functionalizable surface platform with reduced nonspecific protein adsorption from full blood plasma—Material selection and protein immobilization optimization. *Biosens. Bioelectron.* **2009**, *24* (7), 1924−1930.

https://doi.org/10.1021/acssensors.4c00558
ACS Sens. XXXX, XXX, XXX−XXX